2017

# Micro-displacement reconstruction using a laser self-mixing grating interferometer with multiple-diffraction

Dongmei Guo
*University of Wollongong*, dguo@uow.edu.au

Liheng Shi
*Nanjing Normal University*

Yanguang Yu
*University of Wollongong*, yanguang@uow.edu.au

Wei Xia
*Nanjing Normal University*

Ming Wang
*Nanjing Normal University*

## Abstract
In this paper, we demonstrated an improved laser self-mixing grating interferometer (SMGI) with auto-collimation design which can avoid the disturbance from the light feedback of the zero-order diffraction beam. In order to obtain higher optical subdivision, SMGI with multiple-diffraction is implemented. Both theoretical analysis and experimental work show that the proposed system for displacement measurement can achieve high sensitivity and low measurement uncertainty. Using the proposed system, different forms of micro-displacement signals applied on the target (grating) have been reconstructed with accuracy of a few nanometers. The work presented in this paper provides a good way to achieve robust and high precision measurement with compact system configuration.

Research Article | Vol. 25, No. 25 | 11 Dec 2017 | OPTICS EXPRESS 31394
Optics EXPRESS

# Micro-displacement reconstruction using a laser self-mixing grating interferometer with multiple-diffraction

**DONGMEI GUO,[1,2] LIHENG SHI,[1] YANGUANG YU,[2,*] WEI XIA,[1] AND MING WANG[1]**

[1]*Jiangsu Key Laboratory on Opto-Electronic Technology, School of Physics and Technology, Nanjing Normal University, Nanjing 210023, China*
[2]*School of Electrical, Computer and Telecommunications Engineering, University of Wollongong, NSW 2522, Australia*
**yanguang@uow.edu.au*

**Abstract:** In this paper, we demonstrated an improved laser self-mixing grating interferometer (SMGI) with auto-collimation design which can avoid the disturbance from the light feedback of the zero-order diffraction beam. In order to obtain higher optical subdivision, SMGI with multiple-diffraction is implemented. Both theoretical analysis and experimental work show that the proposed system for displacement measurement can achieve high sensitivity and low measurement uncertainty. Using the proposed system, different forms of micro-displacement signals applied on the target (grating) have been reconstructed with accuracy of a few nanometers. The work presented in this paper provides a good way to achieve robust and high precision measurement with compact system configuration.



**OCIS codes:** (120.3180) Interferometry; (280.0280) Remote sensing and sensors; (050.1950) Diffraction gratings.

## References and links

1. C. C. Hsu, C. C. Wu, J. Y. Lee, H. Y. Chen, and H. F. Weng, "Reflection type heterodyne grating interferometry for in-plane displacement measurement," Opt. Commun. **281**(9), 2582–2589 (2008).
2. A. Kimura, W. Gao, Y. Arai, and L. Zeng, "Design and construction of a two-degree-of-freedom linear encoder for nanometric measurement of stage position and straightness," Precis. Eng. **34**(1), 145–155 (2010).
3. S. Donati and M. Norgia, "Self-mixing interferometry for biomedical signals sensing," IEEE J. Sel. Top. Quantum Electron. **20**(2), 104–111 (2014).
4. S. Zhang and W. Holzapfel, *Orthogonal Polarization in Lasers: Physical Phenomena and Engineering Applications* (John Wiley and Sons, 2013).
5. S. Zhang, S. Zhang, L. Sun, and Y. Tan, "Spectrum broadening in optical frequency-shifted feedback of microchip laser," IEEE Photonics Technol. Lett. **28**(14), 1593–1596 (2016).
6. K. Zhu, B. Guo, Y. Lu, S. Zhang, and Y. Tan, "Single-spot two-dimensional displacement measurement based on self-mixing interferometry," Optica **4**(7), 729–735 (2017).
7. M. T. Fathi and S. Donati, "Thickness measurement of transparent plates by a self-mixing interferometer," Opt. Lett. **35**(11), 1844–1846 (2010).
8. Y. Tan, W. Wang, C. Xu, and S. Zhang, "Laser confocal feedback tomography and nano-step height measurement," Sci. Rep. **3**, 2971 (2013).
9. S. Donati, D. Rossi, and M. Norgia, "Single channel self-mixing interferometer measures simultaneously displacement and tilt and yaw angles of a reflective target," IEEE J. Quantum Electron. **51**(12), 1–8 (2015).
10. Y. Tan, S. Zhang, C. Xu, and S. Zhao, "Inspecting and locating foreign body in biological sample by laser confocal feedback technology," Appl. Phys. Lett. **103**(10), 101909 (2013).
11. Y. Fan, Y. Yu, J. Xi, and J. F. Chicharo, "Improving the measurement performance for a self-mixing interferometry-based displacement sensing system," Appl. Opt. **50**(26), 5064–5072 (2011).
12. Y. Tan, S. Zhang, and Y. Zhang, "Laser feedback interferometry based on phase difference of orthogonally polarized lights in external birefringence cavity," Opt. Express **17**(16), 13939–13945 (2009).
13. K. Lin, Y. Yu, J. Xi, H. Li, Q. Guo, J. Tong, and L. Su, "A Fiber-Coupled Self-Mixing Laser Diode for the Measurement of Young's Modulus," Sensors (Basel) **16**(6), 928 (2016).
14. D. Guo, M. Wang, and H. Hao, "Self-mixing grating interferometer: theoretical analysis and experimental observations," Proc. SPIE **9960**, 996019 (2016).
15. D. Guo and M. Wang, "Note: Design of a laser feedback interferometer with double diffraction system," Rev. Sci. Instrum. **86**(9), 096111 (2015).

#309855 https://doi.org/10.1364/OE.25.031394
Journal © 2017 Received 24 Oct 2017; revised 27 Nov 2017; accepted 27 Nov 2017; published 1 Dec 2017

16. J. Y. Lee, H. Y. Chen, C. C. Hsu, and C. C. Wu, "Optical heterodyne grating interferometry for displacement measurement with subnanometric resolution," Sensor Actuat. A-Phys. **137**(1), 185–191 (2007).
17. C. Palmer and E. G. Loewen, *Diffraction Grating Handbook* (Newport Corporation, 2005).
18. F. Cheng and K. C. Fan, "Linear diffraction grating interferometer with high alignment tolerance and high accuracy," Appl. Opt. **50**(22), 4550–4556 (2011).
19. T. Bosch and S. Donati, "Optical feedback interferometry for sensing application," Opt. Eng. **40**(1), 20–27 (2001).
20. W. Xia, M. Wang, Z. Yang, W. Guo, H. Hao, and D. Guo, "High-accuracy sinusoidal phase-modulating self-mixing interferometer using an electro-optic modulator: development and evaluation," Appl. Opt. **52**(4), B52–B59 (2013).

## 1. Introduction

Nano-scale positioning and scanning stages have become increasingly important in nanotechnology applications. To achieve high resolution positioning, the displacements of such stages must be acquired for feedback control of the stage position, which is one of the most important factors influencing the stage performance. Many kinds of sensors have been designed to measure the displacements of stages, such as capacitance transducers and laser interferometers [1]. Optical heterodyne interferometers and grating interferometers are commonly used for displacement sensing in the feedback control system [2]. However, the optical configuration of such interferometers is very complicated and it is not easy to operate because there are many optical components, such as polarizer, polarizing beam splitter, and wave plates in the system.

Self-mixing interference (SMI), owing to its unique compactness, robustness and cost-effectiveness has attracted more and more attention in recent years [3–5]. It has proved to be a powerful tool in the precision measurement of displacement, velocity, thickness, angles and refractive index etc [6–13]. Identical to the conventional two-beam interferometers, the measurement standard of SMI is the laser wavelength $\lambda$. The measurement accuracy is strongly dependent on the laser wavelength stability. However, the laser wavelength can be affected by the optical feedback in SMI, which will cause unavoidable measurement error. Though the optical feedback level is always controlled in a weak level to minimize the wavelength undulation, the influence cannot be neglected in precision measurement. Besides, the variations in temperature, humidity, air pressure and air flow in the environment will lead to deterioration in the measurement accuracy.

By introducing a diffraction grating in SMI, we have reported a novel self-mixing grating interferometer (SMGI) [14, 15]. Theoretical analysis and Experimental results show that the proposed SMGI adopts the grating pitch rather than the wavelength as the measuring standard, removing the measurement error caused by the wavelength undulation and providing better immunity against environmental disturbances. Furthermore, compared to traditional SMI, SMGI system does not require an optical attenuator to control the optical feedback strength due to the limitation of the diffraction efficiency. In our previous work [14, 15], a SMGI with double diffraction system is proposed in which a beam emitted from the laser diode is incident onto a grating perpendicularly and the double diffracted beam returns back to the laser cavity, self-mixing interference effect occurs. However, in addition to the measuring light, the zero-order diffraction beam also returns back to the laser cavity. Although it does not introduce an additional phase change in SMGI signal, it will decrease the signal to noise ratio (SNR) of the signal.

In this paper, we report improved works based on the SMGI system. Firstly, we introduce an improved SMGI system with novel auto-collimation design which makes the overall measurement system more compact and easier to operate. The laser beam is incident onto a reflective holographic grating with a fixed angle which makes the measuring light diffract back along the same path of the incident light and cause self-mixing interference effect. It can avoid the feedback of the zero-order diffraction beam so as to improve the SNR of the SMGI signal. Secondly, the new work makes use of multiple-diffraction to enhance the measurement resolution. The multiple-diffraction is implemented by using a plane mirror to

Optics EXPRESS

make the measuring light reflect and diffract between the mirror and grating for several times. Theoretical analysis is presented and the results coincide with the experimental observations. Thirdly, an application of micro-displacement sensing is presented with high precision by the proposed SMGI system.

## 2. SMGI with auto-collimation design

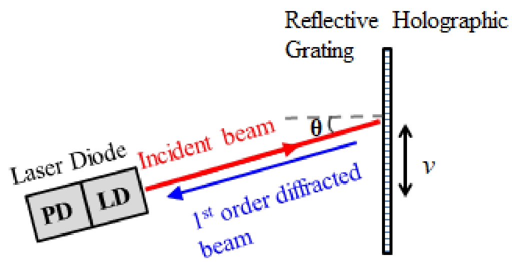


Fig. 1. Schematic diagram of the SMGI with auto-collimation design.

The schematic diagram of the proposed SMGI system with auto-collimation design is shown in Fig. 1. It consists of only a laser diode (wavelength denoted by $\lambda$) and a reflective grating (pitch denoted as $d$). The grating is a sinusoidal amplitude holographic grating that only generates 0th and ± 1st diffraction orders [16]. In addition, ruled gratings suffer from periodic errors, such as ghosting, and relatively high amounts of scattered light, which could negatively affect sensitive measurements. Holographic gratings are designed specially to reduce or eliminate these errors [17]. A beam emitted from the laser diode is incident onto its external target that is a grating. The incident angle of the laser beam denoted by $\theta$ is fixed during the measurement which is determined by

$$\theta = \arcsin\left(\frac{\lambda}{2d}\right). \tag{1}$$

As known, the diffraction law can be written as

$$d(\sin\theta + \sin\beta_q) = q\lambda, \quad q = \pm 1, \pm 2.... \tag{2}$$

Where $\theta$ is the incident angle; $\beta_q$ is the $q$th-order diffraction angles; $q$ is the diffraction order; Substituting Eq. (1) into Eq. (2), we can get

$$\beta_1 = \theta. \tag{3}$$

Thus the 1st-order diffraction beam returns back along the original path of the incident beam as shown in Fig. 1. Self-mixing grating interference occurs when a laser beam is incident onto a reflective holographic grating with a fixed angle $\theta$; the 1st-order diffracted beam is diffracted back into the laser cavity and mixes with the light inside the laser cavity. Due to the limitation of the diffraction efficiency, the intensity of the feedback light to the laser diode can be kept at a weak level. Unlike a traditional SMI, this configuration no longer needs an external attenuator to control the feedback level. Obviously, this design can make the overall system more compact.

When the grating moves with speed as $v$ in vertical direction indicated in Fig. 1, the diffracted light will generate a frequency shift due to Doppler Effect [18]. The frequency shift of the incident light (frequency denoted by $f_0$) and the 1st-order diffracted light (frequency denoted by $f_1$) is expressed as below

$$\Delta f = f_1 - f_0 = 2 f_0 \frac{v}{c} \sin\theta. \tag{4}$$

Optics EXPRESS

Where $c = \lambda f_0$ is the light speed in vacuum. Substituting Eq. (1) into Eq. (4), the frequency shift is simplified as

$$\Delta f = v / d. \tag{5}$$

The phase change due to the movement of the grating can be expressed as

$$\varphi_g(t) = 2\pi\Delta f t = 2\pi x(t) / d. \tag{6}$$

Where $x(t) = vt$ is the displacement of the grating. According to self-mixing effect, a change in light phase will cause the change in both laser intensity and its frequency [19]. The system model for the proposed SMGI can be summarized as follows

$$\omega\tau = \omega_0\tau - C\sin(\omega\tau + \frac{2\pi x(t)}{d} + \arctan\alpha). \tag{7}$$

$$I(t) = I_0[1 + m\cos(\omega\tau + \frac{2\pi x(t)}{d})]. \tag{8}$$

Where $\tau$ is the external cavity round-trip time; $I_0$ is the laser output intensity without feedback; $\omega$ *and* $\omega_0$ are the angular frequency of the laser with and without feedback, respectively; $C$ is the optical feedback strength; $m$ represents the modulation coefficient. Figure 2 is the simulation results of the proposed SMGI with auto-collimation design. Figure 2(a) is the simulated sinusoidal displacement of the grating ($d$ = 0.83μm) with amplitude at 4μm (p-p). Figure 2(b) is the corresponding SMGI signal. It can be seen that each fringe in SMGI corresponds to the change in the grating displacement with $d$, and the inclination of the fringes indicate the direction of the grating movement.

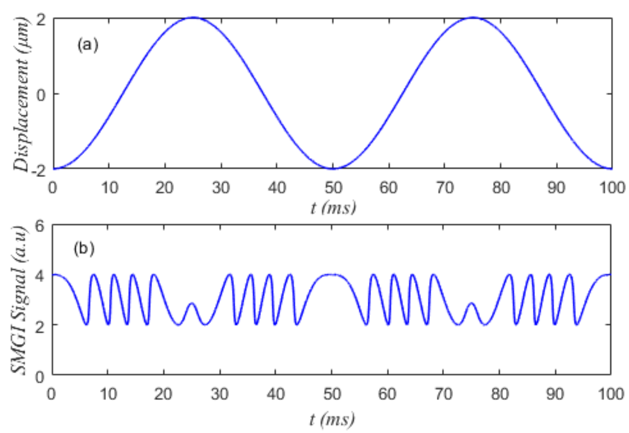


Fig. 2. Simulation results of the SMGI signal (vibration amplitude at 4μm p-p).

Fringe counting method is commonly used for displacement measurement in SMI technology. In traditional SMI configuration, each fringe corresponds to the change in target displacement with $\lambda/2$. But, a fringe change corresponds to the grating pitch $d$ in SMGI. Hence, we say, the measurement resolution for displacement using the proposed SMGI system depends on the grating pitch $d$ but not the laser wavelength $\lambda$. The grating pitch can be manufactured with high accuracy and it does not disturbed by ambient temperature or optical feedback. Hence, the proposed system is more robust compared to the traditional SMI configuration.

Compared with the SMGI system we proposed previously in [14, 15], in this paper, the proposed configuration with auto-collimation design has following advantages: First, it just consists of a laser diode and a diffraction grating, which is more compact. Second, the SNR of the interference signal is higher due to the lower light loss. And the influence of the zero-order back-diffracted light is eliminated. Third, the optical path is easier to adjust. In addition, for further improving the fringe resolution, we introduced a SMGI with multiple-diffraction presented as below.

### 3. Design of a SMGI with multiple-diffraction

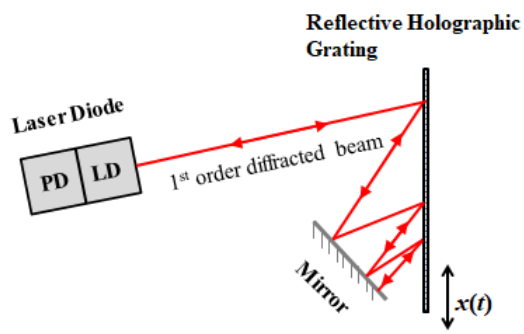


Fig. 3. Schematic diagram of the a SMGI with multiple-diffraction.

Schematic diagram of a SMGI with multiple-diffraction system is shown in Fig. 3. The laser beam from a laser diode is incident onto a reflective holographic grating at a fixed angle. A mirror is fixed at a special position to make the measuring light reflect and diffract between the mirror and grating for several times. Assuming that the number of diffraction times is $N$, the phase change of the SMGI due to the displacement of the grating $x(t)$ is expressed as Eq. (9) due to the grating Doppler Effect

$$\varphi_g(t)=2N\pi x(t)/d. \tag{9}$$

By introducing multiple-diffraction, $1/N$ optical subdivision in SMGI signal can be obtained as follows

$$\left|\Delta\varphi_g(t)\right| = \left|2N\pi\Delta x(t)/d\right| = 2\pi \Leftrightarrow \left|\Delta x(t)\right| = d/N. \tag{10}$$

Here we designed two types of beam path between the mirror and the grating as shown in Fig. 4.

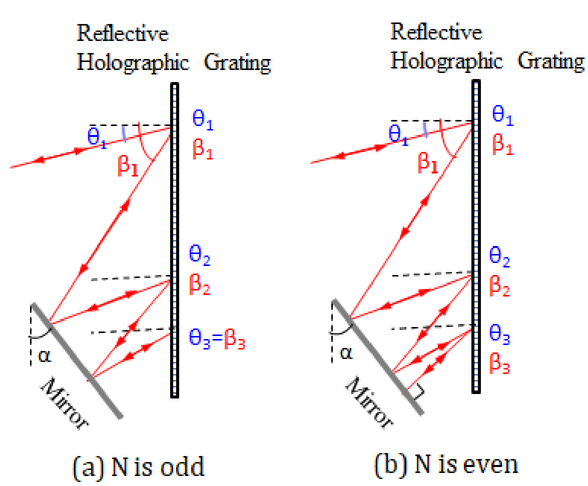


Fig. 4. Schematic diagram of the beam path between the grating and the mirror.

As seen in Fig. 4, a mirror is fixed at a special position and the angle between the mirror and the grating is denoted as $\alpha$. The laser beam is incident on a reflective holographic grating at a fixed angle $\theta_1$. The 1st-order diffracted light hits on the mirror and reflected by the mirror. The reflected light is diffracted by the grating again, and then to the mirror, to the grating, to the mirror, repeatedly. In Fig. 4, $\theta_i$ ($i = 1, 2, 3\ldots n$) is the incident angles, $\beta_i$ ($i = 1, 2, 3\ldots n$) is the diffraction angles. Counting from the first diffraction, the incident angle is $\theta_1$, $\theta_2\ldots\theta_n$ respectively. Similarly, diffraction angle is $\beta_1$, $\beta_2\ldots\beta_n$ respectively.

Here, two types of beam path between the mirror and the grating are designed as shown in Figs. 4(a) and 4(b). In Fig. 4(a), the measuring light is reflected and diffracted between the mirror and grating for several times, finally the measuring light is incident on the grating at the incident angle $\theta_n$ which satisfies the relationship in Eq. (1), and the diffracted light returns back along the same path of the incident light. It returns into the laser cavity and self-mixing grating interference occurs. In this case, the number of diffraction times is $N = 2n-1$. When the angle between the grating and the mirror is fixed as $\alpha$, other angles in Fig. 4(a) can be determined by the following equations

$$\begin{cases} \sin\theta_i + \sin\beta_i = \lambda / d, \quad i = 1, 2..n \\ \theta_{i+1} + \beta_i = 2\alpha, \quad i = 1, 2..n-1 \\ \theta_n = \beta_n = \arcsin(\lambda / 2d). \end{cases} \quad (11)$$

Another type of beam path is shown in Fig. 4(b). The measuring light is reflected and diffracted between the mirror and grating for several times, finally the measuring light hits on the mirror perpendicularly and it returns back along the same path of the incident light and then back into the laser cavity, self-mixing grating interference occurs. In this case, the number of diffraction times is $N = 2n$. When the angle between the grating and the mirror is fixed as $\alpha$, other angles in Fig. 4(b) can be determined by following equations

$$\begin{cases} \sin\theta_i + \sin\beta_i = \lambda / d, \quad i = 1, 2..n \\ \theta_{i+1} + \beta_i = 2\alpha, \quad i = 1, 2..n-1 \\ \beta_n = \alpha. \end{cases} \quad (12)$$

Theoretical analysis shows that by introducing multiple-diffraction, the fringe resolution can be improved to $d/N$. Hence, the smaller grating pitch $d$ used, the more diffraction times introduced, the higher displacement measurement resolution can be achieved.

## 4. Experimental Results

### *4.1 Experimental observations of a laser SMGI with multiple-diffraction*

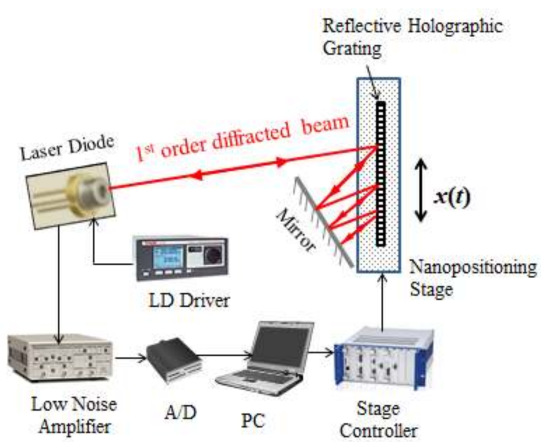


Fig. 5. Experimental Setup of a SMGI with multiple-diffraction.

Experimental observations have been conducted to confirm the validity of the SMGI with multiple-diffraction. Figure 5 is the experimental setup. The output power and wavelength of the laser diode (HL6320G) is 10mW and 635nm respectively. The reflective sinusoidal amplitude holographic grating with pitch 0.83μm is mounted on a 2-D nanopositioning stage (PI, P621.2CD) with closed-loop positioning resolution 0.4nm. The interference signal monitored by the photodetector in the LD package is sent through a low noise voltage amplifier (SR560) and then digitized with a 2 MS/s, 16-bit analog-to-digital converter board (NI 6361).

Figure 6 is the experimental observations of the SMGI signal with multiple-diffraction corresponding to the design of beam path in Fig. 4(a) when $N$ is odd case. During the experiments, the output of the integrated feedback sensor of the nanopositioning stage shows that the grating vibrates at amplitude 3μm peak to peak. Figure 6(a) is the voltage signal corresponding to the grating displacement obtained from the sensor monitor of the stage controller. Figures 6(b)-6(d) are the corresponding SMGI signals with $N = 1, 3, 5$. For these three cases, according to Eq. (9), each interference fringe corresponds to the displacement as 0.83μm, 0.277μm, 0.166μm respectively. The experimental results coincide with the theoretical analysis presented in section 2 for the case with odd $N$.

Figure 7 show the experimental results for the even $N$ case with beam path in Fig. 4(b). During the experiments, the output of the integrated feedback sensor of the nanopositioning stage shows that the grating vibrates at amplitude 3μm peak to peak. Figure 7(a) is the voltage signal corresponding to the grating displacement obtained from the sensor monitor of the stage controller. Figures 7(b)-6(d) are the corresponding SMGI signals with the number of diffraction times $N = 2, 4, 6$. According to Eq. (9), an interference fringe is corresponding to the displacement as 0.415μm, 0.208μm, 0.138μm respectively. And the experimental results again agree well with the theoretical analysis in section 2.

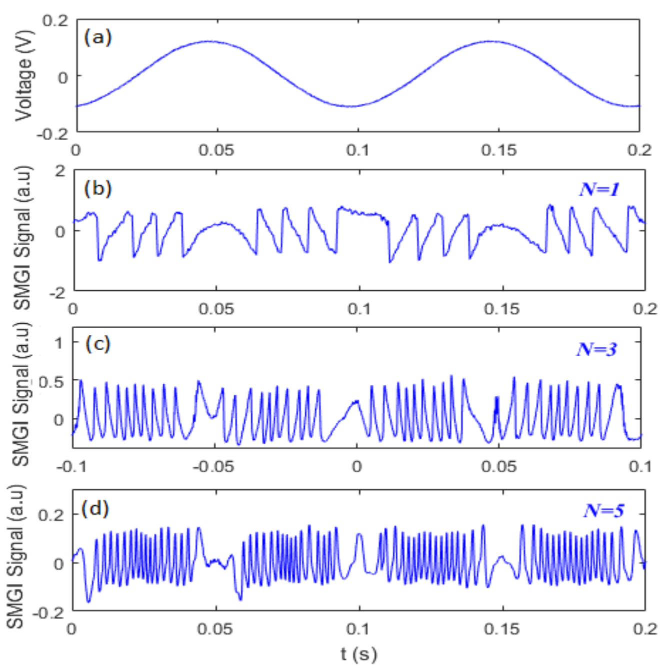


Fig. 6. Experimental observations of the SMGI signal with multiple-diffraction ($N = 1, 3, 5$).

Optics EXPRESS

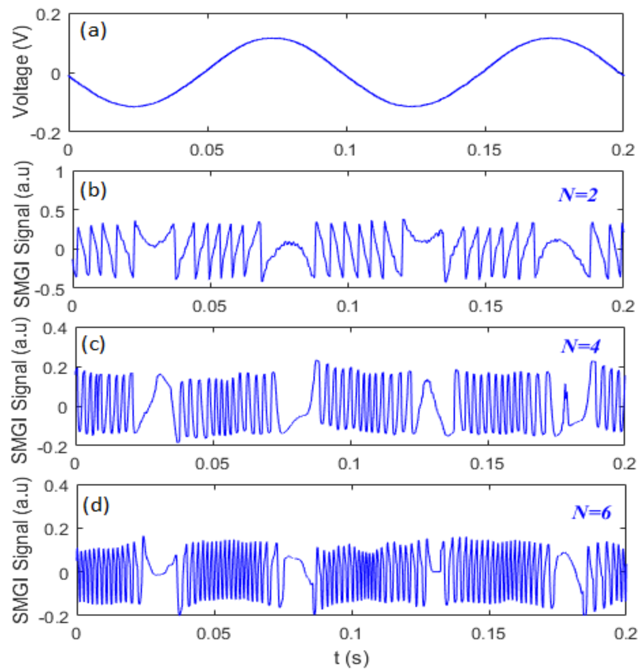


Fig. 7. Experimental observations of the SMGI signal with multiple-diffraction ($N$ = 2, 4, 6).

As indicated in Eq. (10), higher value of $N$ can achieve higher optical subdivision, that is, higher fringe resolution can be gained. However, due to the limitation of the diffraction efficiency, higher $N$ will cause weaker optical intensity back to the laser cavity. Thus, a compromised $N$ should be chosen to guarantee both the fringe resolution and the SNR of the signal. In our work, the highest fringe resolution of $d/6$ has been obtained which we can achieve satisfied SMGI signal quality. This can be further improved by enhancing the laser power and carefully refining the system's electronics and mechanics.

### *4.2 Application of micro-displacement reconstruction*

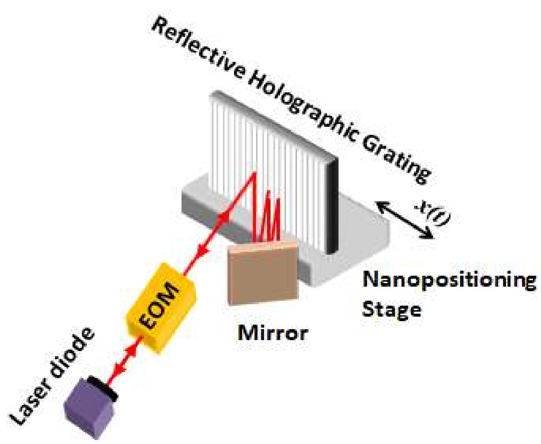


Fig. 8. Displacement measurement configuration using SMGI with multiple-diffraction.

In order to verify the performance of the SMGI with multiple-diffraction, application of micro-displacement reconstruction has been conducted. Here we take the SMGI with diffraction times $N$ = 5 as an example which is shown in Fig. 8. In order to obtain higher

Optics EXPRESS

displacement resolution, an experimentally controlled phase modulation is introduced by an electro-optic modulator (EOM, New Focus 4002) situated between the grating and the laser diode. The angle between the polarization direction of the laser beam and the electro-optically active axis of the EOM is 0°. Then the EOM can provide pure phase modulation with extremely low amplitude modulation. Assuming that the phase modulation function is $asin(2\pi f_m t)$, where $a$ is the modulation depth, $f_m$ is the modulation frequency. Considering that the beam pass through the EOM twice in the external cavity, the modulated SMGI signal can be written as

$$I(t) = I_0\left\{1 + m\cos\left[\phi_0 + \varphi_g(t) + 2a\sin(2\pi f_m t)\right]\right\}. \tag{13}$$

Where $\varphi_0$ is the initial phase of the SMGI signal; $\varphi_g(t)$ is the phase change corresponding to the displacement of the grating. Expanding Eq. (13) in a Fourier series, harmonics at frequency $f_m$ and $2f_m$ have following expressions

$$I(f_m, t) = 2mI_0\sin(\varphi_g(t) + \phi_0)J_1(2a)\sin(2\pi f_m t) = A_1(t)\sin(2\pi f_m t). \tag{14}$$

$$I(2f_m, t) = 2mI_0\cos(\varphi_g(t) + \phi_0)J_2(2a)\cos(4\pi f_m t) = A_2(t)\cos(4\pi f_m t). \tag{15}$$

Where $J_n(2a)$ is the nth-order Bessel function. Then we can calculate the phase variation $\Delta\varphi_g(t)$ from $A_1(t)$ and $A_2(t)$ using the relationship in Eq. (16)

$$\Delta\varphi_g(t) = \Delta\arctan\left[\frac{A_1(t)}{A_2(t)}\cdot\frac{J_2(2a)}{J_1(2a)}\right]. \tag{16}$$

Figure 9 is the signal processing diagram of the phase extraction we have proposed [20]. The phase $\Delta\varphi_g(t)$ obtained from Eq. (16) is wrapped within the region of $-\pi$ and $\pi$ and it requires a phase unwrapping process to return it to a continuous phase signal that is free from $2\pi$ jumps. It mainly includes the following steps: (1) Calculate the difference between the current sample and its directly adjacent left-hand neighbor; (2) If the difference between the two is larger than $+\pi$, then subtract $2\pi$ from this sample and also from all the samples to the right of it; (3) If the difference between the two is smaller than $-\pi$, then add $2\pi$ to this sample and also to all the samples to the right of it. After unwrapping the phase, the displacement of the grating can be determined by

$$\Delta x(t) = \frac{d}{2\pi N}\Delta\varphi_g(t). \tag{17}$$

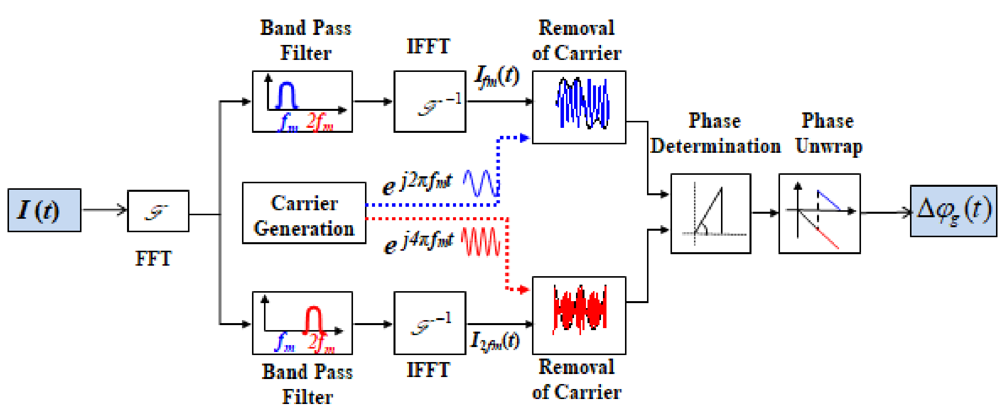


Fig. 9. Signal processing diagram of the phase extraction.

Before taking a measurement, we used a simple method to ensure that the grating plane is parallel to moving axis of the nanopositioning stage. A laser beam is incident onto the grating plane perpendicularly and the zero-order diffracted light returns into the laser cavity. When the stage is moving, if the grating plane is parallel to the moving axis, no interference signal can be observed since the Doppler frequency shift of the zero-order diffractive beam is 0. If the grating plane is not parallel to the moving axis, interference signal can be observed due to the variation in optical path of the feedback light.

By making the grating vibrate at different waveforms, we are able to reconstruct them by the proposed configuration. First, the stage is controlled to move at a sinusoidal form with frequency 10HZ and amplitude (peak to peak) at 600nm, 1000nm, 2000nm and 3000nm respectively. Figure 10 shows the reconstructed displacements. Table 1 shows the displacement amplitude applied on the stage, the results measured by the proposed system and the corresponding measurement errors. Second, the stage is controlled to vibrate at a triangular signal with frequency 10HZ and amplitude (peak to peak) at 200nm, 1000nm and 3000nm respectively. Figure 11 and Table 2 show the related results. From above experimental results, we can see that the proposed SMGI with multiple-diffraction can effectively measure the displacements with high accuracy.

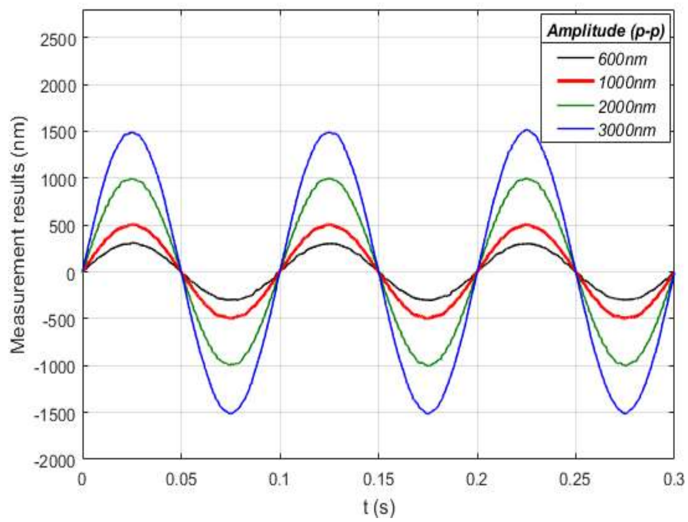


Fig. 10. Reconstructed sinusoidal movements of the grating (10HZ).

**Table 1. Measurement results of the sinusoidal movements**

| Controlled displacement (p-p) (nm) | Measurement results of three periods (nm) (p-p) | | | Maximum Error (nm) |
|---|---|---|---|---|
| | Period 1 | Period 2 | Period 3 | |
| 600 | 604 | 599 | 601 | 4 |
| 1000 | 1005 | 1001 | 998 | 5 |
| 2000 | 2002 | 2000 | 1999 | 2 |
| 3000 | 3000 | 3003 | 2996 | 4 |

Optics EXPRESS

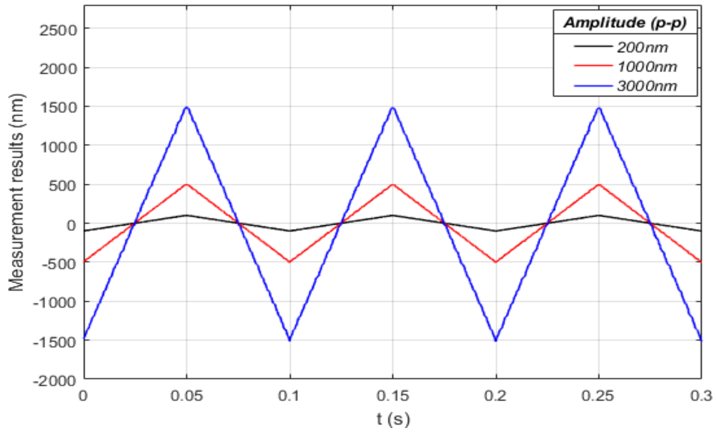


Fig. 11. Reconstructed triangular movements of the grating (10HZ).

**Table 2. Measurement results of the triangular movements**

| Controlled displacement (p-p) (nm) | Measurement results of three periods (nm) (p-p) | | | Maximum Error (nm) |
|---|---|---|---|---|
| | Period 1 | Period 2 | Period 3 | |
| 200 | 206 | 198 | 202 | 6 |
| 1000 | 1002 | 1001 | 998 | 2 |
| 3000 | 3008 | 3004 | 2997 | 8 |

## 5. Discussion

### *5.1 Measurement sensitivity*

Based on Eq. (9), the measurement sensitivity of our system can be written as

$$s = \frac{d\varphi_g}{dx} = \frac{2N\pi}{d}. \tag{18}$$

It is obvious that the higher number of the diffraction times $N$, the smaller grating pitch $d$ used in the optical system, the higher measurement sensitivity $s$ will be achieved. Assuming that the grating pitch $d$ is 0.83μm, the measurement sensitivity $s$ is 0.43°/nm when $N = 1$. However, the measurement sensitivity can be improved to 2.58°/nm when $N = 6$.

### *5.2 Measurement uncertainty*

The uncertainty of the grating pitch $|\Delta d|$ and phase $|\Delta\varphi_g|$ will influence the measurement accuracy of the proposed system. The error of the grating pitch could be coming from the tolerance and the non-uniformity of the grating. The uncertainty of the extracted phase may come from the electrical noise, environment vibration, and the airstream turbulence. The phase fluctuation could be maintained less than 1° under well-controlled conditions, such as the active-isolated table, electric isolation system, and the shelter. From Eq. (17), the theoretical measurement error of the SMGI with multiple-diffraction is given by the following expression

$$|\Delta x| = \frac{d}{2N\pi}|\Delta\varphi_g| + \frac{\varphi_g}{2N\pi}|\Delta d|. \tag{19}$$

Assuming that $|\Delta d|$ and $|\Delta\varphi_g|$ are better than 1nm and 1° during the measurement, the theoretical error could be better than 3.5nm at the displacement of 1μm when $N = 1$. However, the maximum theoretical error decreases to 1.6nm when $N = 6$. It is obvious that the more times the measuring light diffracted, the higher measurement accuracy will be achieved in the measurement.

### 5.3 Measurement Speed

In the measurement system we proposed, the measurement speed was limited mainly by two factors. One is the modulation frequency of the EOM $f_m$ and another is the sampling rate of the A/D convertor $f_s$. From Fig. 9, it can be seen that the phase is extracted from the first harmonic and the second harmonic of the modulated SMGI signal. The sampling rate $f_s$ required in the experiments should satisfy the relationship $f_s > 2f_m$ according to the Nyquist theorem. As for the modulation frequency $f_m$, the occurrence of measurement error due to band overlapping in the frequency domain should be considered. As shown in Eq. (14) and Eq. (15), $A_1$ (t) and $A_2$ (t) have instantaneous frequency $d\varphi_g/(2\pi dt)$ which is proportional to the speed of the grating. Therefore, the first harmonic and the second harmonic centered at $f_m$ and $2f_m$ present a spectral width proportional to the maximum velocity of the external target. To avoid overlapping problems, $\varphi_g$ can only have spectral components limit to $f_m$ /2 which can be expressed as

$$\frac{d\varphi_g}{2\pi dt} \le \frac{f_m}{2}. \tag{20}$$

Substituting Eq. (9) into Eq. (20), the following relationship can be obtained

$$v_{\max} = f_m d / 2N. \tag{21}$$

From Eq. (21) we can see that the maximum measurable velocity $v_{max}$ is determined by the modulation frequency $f_m$ when the sampling rate of the A/D convertor is high enough.

### 5.4 Measurement Range

The maximum measurable amplitude of the proposed system is related to the maximum measurable velocity and the grating size. Assuming that the grating vibrates as $x = x_0\sin(2\pi f_0 t)$, where $x_0$ and $f_0$ are the amplitude and frequency of the movement. From Eq. (21), the maximum measurable amplitude $x_{0\max}$ can be calculated as

$$x_{0\max} = f_m d / 4\pi N f_0. \tag{22}$$

Therefore, the maximum measurable amplitude of the proposed system mainly depends on two factors, one is the grating size and the other is also the modulation frequency $f_m$.

The minimum measurable amplitude of the proposed system, also called the measurement resolution, is limited by the precision of the phase extraction and the error of the grating pitch. Figure 12 is the measurement result of the sinusoidal displacement with amplitude 5nm (p-p) when $N$ = 5. It can be seen that the system proposed can discriminate displacement under 10nm.

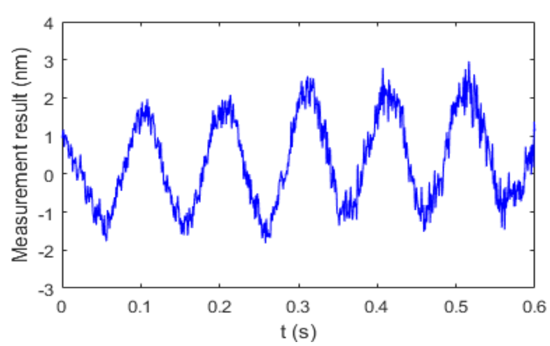


Fig. 12. Measurement result of the grating displacement with amplitude 5nm (p-p).

Optics EXPRESS

## 6. Conclusion

SMGI adopts the grating pitch rather than the wavelength as the measurement standard, removing the measurement error caused by the wavelength undulation and providing better immunity against environmental disturbances. In this paper we demonstrate an improved SMGI with auto-collimation design which can avoid the feedback of the zero-order diffraction beam. And the configuration is more compact and easier to operate than the SMGI we proposed previously. Furthermore, we introduced multiple-diffraction to the proposed system to achieve high measurement sensitivity and low measurement uncertainty. Micro-displacements in different forms have been successfully reconstructed with high accuracy to verify the performance of the proposed system. This work provides a potential displacement sensor with high resolution, simple mechanical structure, and good reliability.

## Funding

National Natural Science Foundation of China (NSFC) (51405240, 51775283); Major Project of Natural Science Foundation of Jiangsu Higher Education Institutions of China (17KJA510002); Natural Science Foundation of Jiangsu Province of China (BK20161559).